Lateral undulation of the bendable body of a gecko-inspired robot for energy-efficient inclined surface climbing

Worasuchad Haomachai, Donghao Shao, Wei Wang, Aihong Ji, Zhendong Dai, Poramate Manoonpong*

***Abstract*—Sprawling posture animals with their bendable spine, such as salamanders, and geckos, can perform agile and versatile locomotion including walking, swimming, and climbing. Therefore, several roboticists have used them as templates for robot designs to investigate and generate efficient locomotion. Typically, walking and/or swimming abilities are realized by salamander-inspired robots with a bendable body, whereas climbing ability is achieved on gecko-inspired robots with an over-simplified fixed body. In this study, we propose optimal bendable body design with three degrees of freedom (DOFs). Its implementation on a sprawling posture robot is inspired by geckos for climbing enhancement. The robot leg and body movements are coordinated and driven by central pattern generator (CPG)-based neural control. As a consequence, the robot can climb using a combination of trot gait and lateral undulation of the bendable body with a C-shaped standing wave. Through the real robot experiments on a 3D force measuring platform, we demonstrate that, due to the dynamics of the bendable body movement, the robot can gain higher medio–lateral (F_x) ground reaction forces (GRFs) at its front legs as well as anterior–posterior (F_y) GRFs at its hind legs to increase the bending angular momentum (L_{AM}). This results in 52% and 54% reduced energy consumptions during climbing on steeper inclined solid and soft surfaces, respectively, compared to climbing with a fixed body. To this end, the study provides a basis for developing sprawling posture robots with a bendable body and neural control for energy-efficient inclined surface climbing with a possible extension towards agile and versatile locomotion, such as sprawling posture animals.**

***Keywords*—climbing robot, sprawling locomotion, bendable body, lateral undulation, central pattern generator, neural control, bending angular momentum**

I. Introduction

Sprawling animals, such as geckos and salamanders, have a bendable spine that can bend their trunk to coordinate with their limb movements during locomotion. The coordination plays a crucial role in obtaining agile locomotor capabilities (e.g., acceleration of locomotion [1] [2] [3], flexible trajectories during turning [4], stabilization of the body [5] [6], energy efficiency [7]) and versatile locomotor behaviors including walking, swimming, and climbing. Particularly, geckos not only perform various locomotion modes but also display the standing and traveling waves of lateral undulation patterns during slow-speed trotting and high-speed running, respectively. They achieve this by altering the angular velocity of the spine and limb joints, which also enhance locomotion stability [8]. Therefore, many researchers have investigated sprawling locomotion with lateral spine movement to develop robots that approach animal locomotor skills.

To date, there are two main streamlines of sprawling posture robot development. The first one focuses on the development of sprawling robots inspired by salamanders for terrestrial walking [9], [10], aquatic stepping [11], and/or swimming [12], [13], [14]. Modern sprawling robots, like Salamandra robotica [12], [13] and Pleurobot [14], can achieve not only multimodal locomotion modes but a smooth transition from swimming in water to walking on a non inclined surface and vice versa. One of key ingredients underlying the achievement is the use of a bendable segmented spine with 8-11 active joints. The spine basically improves robot locomotion through lateral undulation. The spine is designed and optimized based on the cineradiographic data from different salamander locomotion modes.

Parallel to the first streamline, the second one focuses on the development of sprawling robots inspired by geckos for terrestrial walking and/or climbing. Most gecko-inspired robots[1] mainly focus on special foot structure design [15] and the use of directional or non-directional dry adhesive materials for climbing smooth inclined and vertical surfaces [15], [16], [17], [18], [19], [20], [21]. Although they exhibit impressive climbing ability, none of them have exploited the essential role of the lateral undulation of a bendable body as realized in salamander-inspired robots and found in geckos [22] for efficient locomotion. This is because they are typically designed with an over-simplified fixed body. From this point of view, in this study we propose an optimal bendable body design with three DOFs and demonstrate its implementation on a gecko-inspired robot, Slalom (Fig. 1) for climbing enhancement on inclined surfaces. The body was designed to closely match the body lateral movement of Gekko geckos. Slalom, with its bendable body and four legs, has a total of 19 joints (i.e., three joints for the body and four for each leg), which are coordinated and driven by central pattern generator (CPG)-based neural control. The main contributions of this study include: i) a gecko-inspired bendable body design and movement for energy-efficient climbing inclined solid and soft surfaces; ii) CPG-based neural control for bendable body and leg coordination to achieve a trot gait, lateral body undulation with a C-shaped standing wave, and their combination; iii) real robot climbing experiments at different movement frequencies under different inclined angles, as well as a comparison

W. Haomachai, D. Shao, W. Wang, A. Ji, Z. Dai and P. Manoonpong are with the Institute of Bio-inspired Structure and Surface Engineering, College of Mechanical and Electrical Engineering, Nanjing University of Aeronautics and Astronautics, Nanjing, China. P. Manoonpong is also with Bio-inspired Robotics & Neural Engineering Lab, School of Information Science & Technology, Vidyasirimedhi Institute of Science & Technology, Rayong, Thailand and Embodied AI & Neurorobotics Lab, SDU Biorobotics, Mærsk Mc-Kinney Møller Institute, University of Southern Denmark, Odense, Denmark. All correspondence should be addressed to *P. Manoonpong, (poma@nuaa.edu.cn, poramate.m@vistec.ac.th)

[1]Note that, the main difference between salamander and gecko-like robots is described in the discussion section.

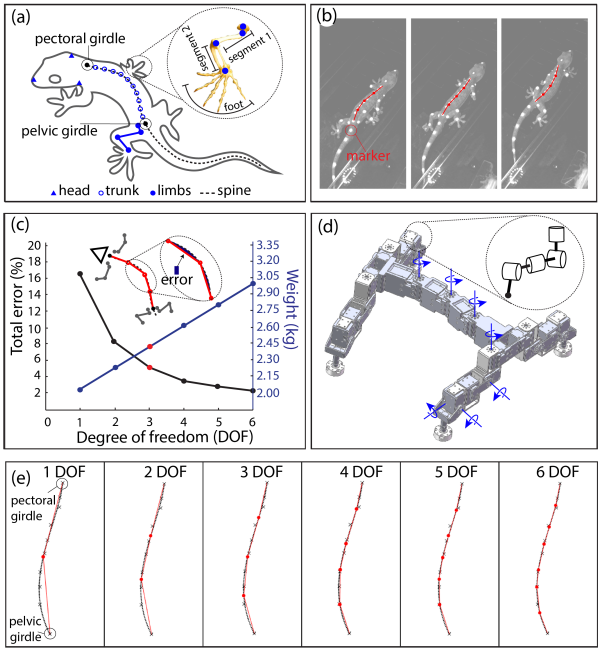

Fig. 1. The robot's spine was optimally designed to match its biological counterpart's kinematics during locomotion. We used a high-speed camera to record the Gekko gecko and the resulting three-dimensional kinematics of the skeletal structure to design the robot's body. (a) Animal morphology composed of the head, spine, and four limbs. (b) Snapshot of high-speed video of gecko movement. The white points on the gecko are reference markers for tracking the movement of its skeleton. (c) An error area between the observed trunk bending in the Gecko and the segmented line with different joint numbers were considered. The resulting number of joints (three, indicated by red point) was selected as a trade-off between the accuracy of the approximation and the minimal number of joints. Robot weight was estimated as a function of the DOFs. The robot weight was 7%, 14%, or 22% heavier than the three DOFs, when four, five, or six DOFs were selected, respectively. Likewise, the power consumption increased to 10%, 21%, 32%. (d) According to our design methodology, Slalom is constructed with a 3-DOF body and four DOFs per leg. (e) Different DOFs with symmetrical positions. Their segmented line (red line) is compared with the curvature of the gecko's body (black curve).

of climbing performance with and without the lateral body undulation, and iv) ground reaction force and bending angular momentum analysis under body movement dynamics.

II. Gecko-inspired Design Methodology

A. Gecko experiments and data processing

The structural design of our robot Slalom is based on the Gekko gecko which exhibits agile movement for flexible and efficient walking, running, and particularly climbing. Its morphology is composed of a head, an elongated body (trunk and tail) and four limbs located at the pectoral and pelvic girdles (Fig. 1a). The spine and leg movements during locomotion were determined from experimental videos recorded using a high-speed camera (Olympus iSpeed-3, 1280-pixel $\times$ 1024-pixel resolution, a frame rate of 500 Hz). Before each trial, the reference points were marked on the gecko's spine, head, and legs using 29 infrared reflective markers (Fig. 1b). The white circle markers were placed on the legs (12 markers), trunk (ten markers), tail (five markers), and head (two markers). The animal experiments were performed as per the Guidelines for Laboratory Animal Management in China. The experimental procedures were approved by the Jiangsu Association for Laboratory Animal Science (Jiangsu, China, approved file no. 2019-152).

The recorded videos were used to track the movement of the gecko skeleton during forward movement. For this purpose, a motion tracking software based on MATLAB (MATLAB R2019b, MathWorks, Inc.) was developed and used. The top and side views were digitized at a frame rate of 120 Hz. The body posture dataset was then used to guide an evaluation with the optimal segmentation of the robot's body (i.e., the minimum number of joints), and their placement was defined as equidistant. A comparison of the animal and robot spine structures is shown in Figs. 1a and 1d, respectively.

B. Gecko-inspired bendable body and limb design

The recorded data for the axial movements of the gecko show that during steady-state locomotion, the gecko undulated mainly in the transverse plane; bending in the sagittal plane was in a very small range [4]. This reduces the problem of designing the robot body for optimal segmentation in the transverse plane.

Each snapshot of the gecko body was represented as ten marker points in Cartesian coordinates. These points were converted to a continuous curve as the hypothetical midline of the body (body interpolation). The conversion was performed using a polynomial curve fitting function (polyfit) in MATLAB, with a fourth-degree polynomial equation. The starting point of the midline was defined as the tip of the body (the pectoral girdle) and the endpoint was defined as the end of the body (the pelvic girdle). The midline was then resampled to 100 equidistant points, which are shown by the black line in Fig. 1e. It is important to note here that the average length of all the curves in the dataset was used to define the length of the gecko's body.

To identify the best fit using the least-squares method, we performed several iterations with different numbers of joints between the defined positions of the pectoral and pelvic regions on the midline. Arbitrarily, 1-6 joints with equal distances between them were applied to different iterations (Fig. 1e). To evaluate how well the number of joints with their symmetrical positions could reproduce the curvature of the gecko's body, we introduced an error metric as the sum of the area between the segmented line and each curve in the dataset of the gecko postures (Fig. 1c).

As expected, the greater the number of joints, the better the segmented line can capture the shapes of the gecko's body during locomotion (Fig. 1c). The approximate exponential convergence of the total error value facilitated the selection of three joints, which we considered as a good trade-off based on the geometry as well as the resulting length and weight of the robot (Figs. 1c and 1d). Consequently, this optimal number with its symmetrical position allows Slalom to imitate the bending of the gecko's body in different postures during locomotion. The robot body is scaled up by increasing the size related to the ratio of the gecko's body and the size of the motors. Consequently, the final size of Slalom's body is larger than that of the gecko with a scale factor of 1:3.33.

The limbs of the gecko consist of two main segments (Fig. 1a). In our previous work [15], we described these two segments as a four-DOF limb with three DOFs at the shoulder/hip joint and one at the elbow/knee (Figs. 1d and 2c). The analysis of the kinematics suggests that all four DOFs were used during locomotion. Thus, they were all included in Slalom. Adjoining the two main segments of the limb is the foot, which has a highly complex structure with multiple compliant toes. Here, we consider the foot as a simple structure composed of two layers. The top part was built by aluminum and consists of a ball joint that provides the foot with three passive DOFs (passive wrist/ankle, Fig. 2c). This allows for the passive self-adjustment of the foot to the substrate. However, the passive movement is limited by a mechanical stopper around the ball joint. When the foot pillar reaches the stopper, it naturally changes from a freely moving part to a fixed part [15]. The range of the allowed angle movement of the pillar is ± 30 degree. The bottom layer is attached by a soft material EPDM rubber sheet for surface adhesion. Taken together, Slalom's forelimbs and hindlimbs follow the same design methodology and can perform their movements close to the gecko limb movements.

III. Slalom, A gecko-inspired robot

A. Robot hardware setup

Slalom has four identical limbs, each of which has four joints (Fig. 2c). The joints 1-3 correspond to the shoulder/hip joint of each front/hind leg. The joint 1 enables forward (+) and backward (-) movements, the joint 2 enables elevation (+) and depression (-) of the leg, and the joint 3 enables the attachment (-) and detachment (+) of the foot. The joint 4 corresponds to the elbow/knee joint of each front/hind leg; it enables the extension (+) and flexion (-) of the foot. The maximum and minimum ranges of the joint movements of the legs are shown in Fig. 2b. The body of Slalom consists of three joints in accordance with the optimal number of joints for the body. These body joints (BJ) can rotate around the vertical axis in a range between ± 60 degrees. It stays at zero degree during locomotion when the robot moves with a fixed body or rotates periodically when the robot moves with a bendable body. Slalom has 19 active joints in total (four at each leg, three at the body) and its weight is $2.45\,\mathrm{kg}$.

For the actuation, we chose Dynamixel XM430-W350 servomotors from ROBOTIS, Inc., as they offer an excellent trade-off featuring a fairly high torque-mass ratio (4.1 Nm of stall torque at 82g), maximum no-load speed of 46 rpm and positional accuracy (0.008 resolution) at a reasonable price. Neural control (described below) is implemented based on a robot operating system (ROS Kinetic) to control the actuators. This control system is installed on an external computer and handles the low-level communication with the servomotors through an RS-485 interface at 4 Mbps. We are able to send motor position commands and receive feedback between the servomotors at a maximum rate of 1kHz. The electrical power supply for all servomotors is provided by the adapter with a voltage regulator producing a stable 12V supply. The entire mechanical structure of Slalom is created using 3D-printing with Polylactic acid (PLA).

B. CPG-based neural control

This robot uses CPG-based neural control that can generate basic locomotion patterns. The entire neural control system has three components: i) a CPG mechanism with neuromodulation for generating different periodic signals and shunting inhibition for altering body joint movements, ii) neural CPG post-processing for shaping the CPG signals to obtain smooth joint movements, and iii) motor neurons for sending final motor position commands to all joints of Slalom.

The structure of this control system is based on our previous work [23] in which a chaotic CPG is modified to a simpler CPG mechanism with neuromodulation. All the neurons of the control system (Fig. 2a) are discrete-time non-spiking neurons and their update frequency is approximately 10 Hz. The activity a_i of each neuron develops according to the following equation:

$$a_i(t) = \sum_{j=1}^{n} W_{ij} \cdot o_j(t-1) + B_i, \quad i = 1, ..., n., \qquad (1)$$

where n denotes the number of neurons, B_i an internal bias term along with a stationary input to neuron i, and W_{ij} the synaptic strength of the connection from neuron j to neuron i. The output of the neuron is calculated using a hyperbolic tangent ($tanh$) activation function (i.e., $o_i = tanh(a_i)$). Therefore, the value of o_i is between -1 and 1.

The CPG is a recurrent neural network with two fully connected neurons (Fig. 2a). This main network generates periodic signals for locomotion. Recurrent weights between both neurons are determined by $W_{12} = 0.18 + MI, W_{21} = -W_{12}$, whereas weights $W_{11,22}$ are set to 1.4. MI is an extrinsic modulatory input used to generate different stride frequencies of moving gait. This parameter setup with $MI = 0.08$ results in the lowest stride frequency of $0.10\,\mathrm{Hz}$. Increasing MI will increase the stride frequency of moving (Fig. 3a). However, MI is limited at 0.26 (stride frequency of $0.25\,\mathrm{Hz}$) because the motor of Slalom cannot properly follow the high driving frequency. The investigation of Slalom climbing on inclined surfaces using this CPG shows that its moving speed is proportional to the value of MI; i.e., increasing MI leads to an increase in fast moving speed (Fig. 3d). In addition, Slalom uses the same gait (trot gait) at different values of MI in our study.

The outputs of the CPG (c_i) are passed to the motor neurons through both shunting inhibition and CPG postprocessing (Fig. 2a). The shunting inhibition neuron (SI) is inspired by neurophysiological findings [24]. The neuron receives one inhibitory input (I) and one excitatory input from the CPG neuron 1 (c_1). We manually control the inhibitory input by setting it to either 0 (inactive) or 1 (active) (i.e., $I = 1$ results in the shunting inhibition neuron being inhibited) and the SI is stimulated by receiving the excitatory input. When the inhibitory and excitatory inputs are stimulated simultaneously, the output of the CPG leaks out before it reaches the motor neurons. However, when the inhibitory input is not stimulated ($I = 0$), the output of the CPG is directly sent to the motor neurons (body joints, $BJ_{1,2,3}$). It indicates that the robot moves with a bendable body when I is set to 0 while $I = 1$ is

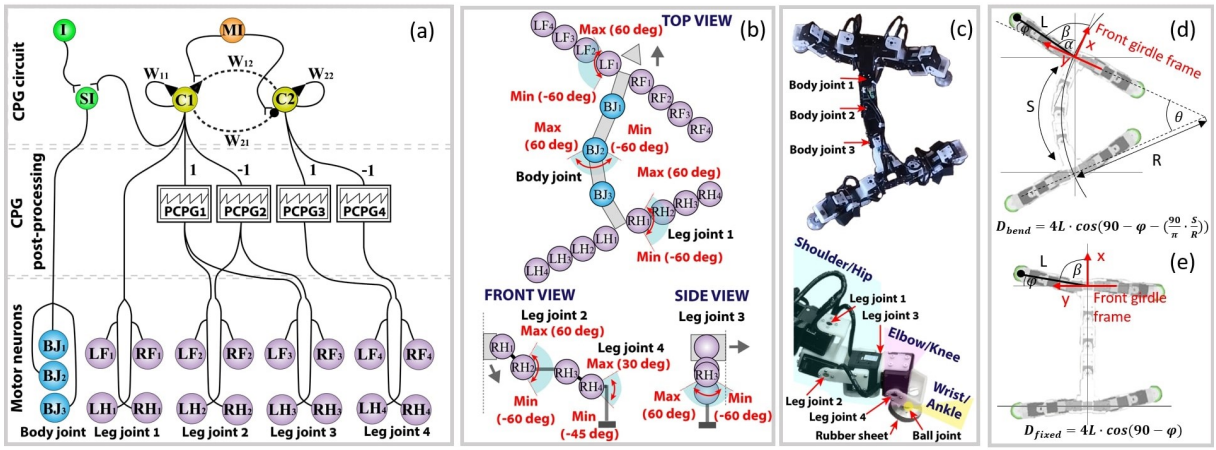

Fig. 2. Architecture of the simplified CPG-based controller. (a) Neural circuit for controlling the gecko-inspired robot. (b) Location of the motor neurons on the robot and their movements. Minimum and maximum angles of the body joints, leg joint 1, leg joint 2, leg joint 3 and leg joint 4. (c) Example of components at the body joints and the left hind leg (LH). (d), (e) Geometrical models of the bendable and fixed bodies. The models can be used to analyze the energy efficiency improvement based on a stride length of the bendable robot body (D_{bend}) compared with the fixed robot body (D_{fixed}). φ is the angle between the foot location and the y-axis of the girdle frame at the beginning of each stride (i.e., 17 degrees). R is the bending radius of the bendable body (i.e., 41.7 cm). L is the leg length (i.e., 17.3 cm). S is the body length (i.e., 35 cm). According to the parameter values obtained from the real robot movements driven by the neural control, D_{bend} is approximately 2.24 times larger than D_{fixed}. The bendable-body robot treaded longer than the fixed-body robot during each stride. Therefore, the cost of transport (COT) of the bendable-body robot was lower than that of the fixed-body robot ($\text{COT}_{bend} \cong \frac{COT_{fixed}}{2.24}$, assuming that both robot configurations have the same mess (m) and almost the same energy usage (E)). The COT formula is shown in section IV. D_{bend} and D_{fixed} derivation formulae can be accessed at https://bit.ly/3fXxLjH. Our robot climbing experimental observations (Fig. 5) followed COT estimations.

for a fixed body. The model of the shunting inhibition neural unit is described by:

$$SI(t) = (1 - I) \cdot c_1(t). \tag{2}$$

The CPG post-processing (PCPG) units receive two different input signals consisting of the original and inverse of the CPG output. For instance, the first PCPG unit ($PCPG_1$) directly receives the CPG output while the second PCPG unit ($PCPG_2$) is given by a multiplication of -1 and the output of CPG (inverted CPG output). The post-processing units shape the CPG signals to the asymmetry of ascending and descending slopes (Fig. 3c) as follows. First, the input signals are transformed by the units which produce the step function outputs (Equation 3) with high (1) or low (0) values. Second, the high and low outputs are converted into continuous signals with exponentially ascending and dramatically descending slopes, respectively. The conversion is done as follows:

$$f(c_i(t)) = \begin{cases} 1, & \text{if } -0.87 < c_i(t) < 0.87 \quad \text{and} \quad \frac{\partial c_i(t)}{\partial t} > 0, \\ 0, & \text{otherwise,} \end{cases} \tag{3}$$

$$PCPG_n = f(c_i(t)) \cdot [-1^{(n+1)} \cdot c_i(t)], \tag{4}$$

where n denotes the number of PCPG units and c_i is the outputs of CPG neuron i. According to this, the post-processing CPG outputs are scaled to the range between -1.0 and 1.0. It should be noted that different frequencies of the CPG generate different ascending slopes (Fig. 3c).

The outputs of the post-processing CPG units are directly sent to the motor neurons of the leg joint 2, 3, and 4. The shunting inhibition and CPG outputs are directly sent to the motor neurons of the body joints and leg joint 1, respectively (Fig. 2a). The diagonal joints receive an identical signal, whereas the other diagonal joints receive a $90°$ phase-shifted signal. This setup leads to biologically inspired leg coordination since the legs on each side perform phase-shifted movements of the same frequency [25]. The frequency of the signals is defined by MI of the CPG. Figure 3d illustrates four leg movements during moving forward from low to high frequencies. Slalom shows a trot gait in which the swing and stance phases of the diagonal legs occur simultaneously. The C++ code of the CPG-based control can be accessed from https://bit.ly/3fXxLjH.

IV. Experimental Validation of Slalom

To verify the locomotor abilities of our robot in this design, we carried out a series of experiments that compared the locomotion of the robot with the lateral undulation of the body (bendable body) and the absence of lateral body movement (fixed body). We used the cost of transport (COT), robot speed, and slope angle for our validation. In addition, the ground reaction force and bending angular momentum were analyzed to verify the effect of the bendable body on the ability to climb an inclined surface.

A. Experimental set-up for robot experiments

In this study, the robot was built based on the Gekko gecko and tested in the real environment. Five main experiments were conducted for different stride frequencies of $0.10, 0.15, 0.19, 0.22, 0.25$ Hz to study the robot performance when climbing different slope angles $(0, 15, 20, 25, 30$ degrees). The fastest stride frequency was limited to 0.25 Hz owing to hardware limitations. The experimental data was recorded for 10 trials while traversing a 1 m distance. We structured the slope into two layers: the top layer employed

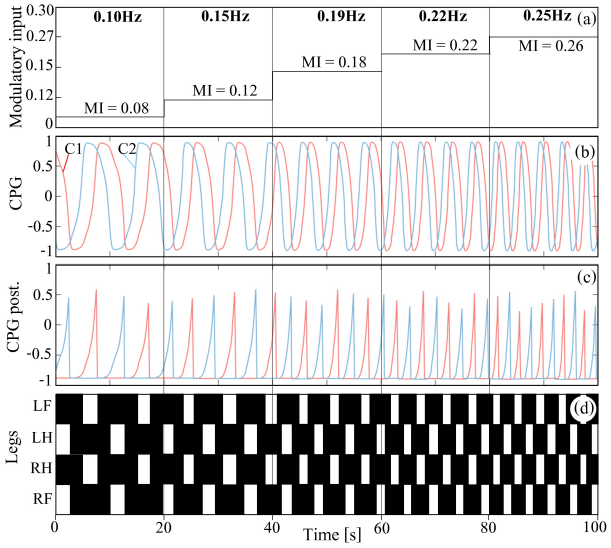

Fig. 3. Examples of trot gait generated by the neural control at five different stride frequencies. (a) Increasing the CPG output frequency trough MI. (b) The CPG output signals. (c) The CPG post-processing output signals. (d) Gait diagram. The black and white areas indicate the stance and swing phases, respectively.

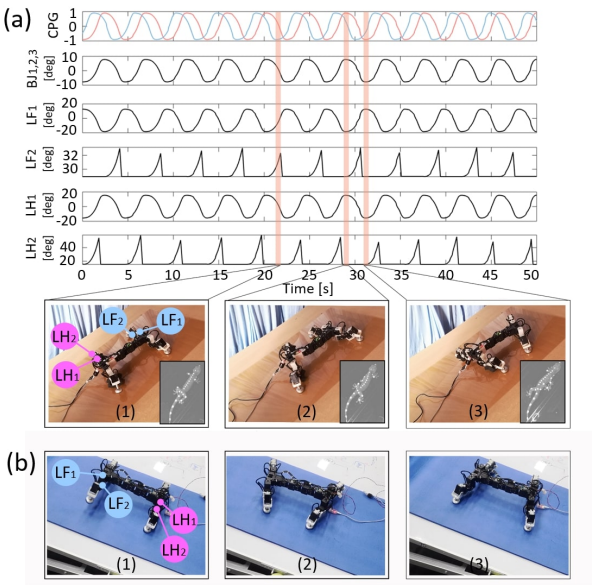

Fig. 4. Example of Slalom locomotion with the bendable body on solid and soft inclined surfaces. (a) The top graph shows the CPG output signals. The other graphs show the joint angles of the body ($BJ_{1,2,3}$, see Fig. 2b), left front ($LF_{1,2}$, see Fig. 2b), and left hind ($LH_{1,2}$, see Fig. 2b). The snapshots below illustrate the postures of the robot and gecko during climbing on an inclined solid surface. (b) The snapshots depict the robotic postures while climbing a soft inclined surface. A video of the experiments can be seen at http://www.manoonpong.com/Slalom/Video1.mp4.

either an acrylic sheet or a foam mat (stiffness of 5 N/mm) as solid or soft climbing surface, respectively and the bottom layer was built with plywood for structural support. The dimension of the slope was 1 m $\times$ 1.5 m.

COT was calculated using the equation COT = E/mgd [26]. E denotes the energy consumed during locomotion, which was calculated using the servo motor embedded sensors. These sensors measured the power consumed by the 19 Slalom servo motors. m, g, and d denote the robot mass (2.45 kg), acceleration due to gravity (9.81 m/s^2), and displacement (1 m), respectively.

B. Robot climbing experiments

This climbing experiments evaluated energy efficiency while moving forward at different solid and soft inclined surfaces with bendable and fixed-body modes. During locomotion, the CPG-based control generated the trot gait. For the bendable body, the gait involves the body oscillation with a C-shaped standing wave that is well-coordinated with the limbs. On solid slopes, different speeds ($0.10, 0.15, 0.19, 0.22,$ and 0.25 Hz) were investigated, whereas on soft slopes, only the most energy-efficient climbing speed (0.25 Hz) realized from solid slope climbing was investigated.

Figure 4a shows an example of the CPG-based control signals during climbing with the bendable body and a stride frequency of 0.25 Hz on the 15-degree solid slope. It should be noted that the signals of the diagonal legs are identical. For instance, the signal of the left front joint 1 (LF_1) is equal to that of the right hind joint 1 (RH_1), and the right front joint 2 (RF_2) and the left hind joint 2 (LH_2) also have the same signal. Furthermore, in each local leg, the signals of both joints 3 and 4 are similar to that of joint 2 but with different amplitudes. Such control strategies were applied while climbing on soft slopes. Snapshots of Fig. 4a depict a 15-degree climbing by the robot on a solid inclined surface, which corresponds to the red areas of the control signals. Photo 1 illustrates the swing phase in which the body joints reached the middle position while rotating from the right side to the left; the elevation of LF_2 and RH_2 was observed, while RF_2 and LH_2 stayed on the ground. Photo 2 shows the stance phase in which the body flexion appeared as a C-shaped standing wave on the right side while all the limbs stayed on the ground. Photo 3 shows the robot performing the opposite C-shaped body flexion during the stance phase. Similar climbing behavior was observed on a 15-degree soft inclined surface (Fig. 4b).

The results of climbing experiments (Fig. 5), show that the COT tends to decrease when the frequency is increased for each solid slope angle. For instance, for the fixed body at a slope with 25 degrees, the robot consumes a COT of approximately 172 at 0.10 Hz, and then begins a sharp downward trend to approximately $137, 109, 94$, and 84 when the frequency is increased to $0.15, 0.19, 0.22$, and 0.25 Hz, respectively. The COT also tends to a similar direction to that the bendable body. It is clear that this solid-slope climbing experiment provided a stride frequency of 0.25 Hz, which consumed the lowest COT on each slope, and consequently it was defined as the optimal moving speed. This frequency was employed in the soft inclined surface climbing experiment (Fig. 5). While the bendable-body robot climbed solid and soft surfaces inclined up to 30 and 25 degrees, respectively, the fixed-body robot climbed those inclined up to 25 and 20 degrees, respectively.

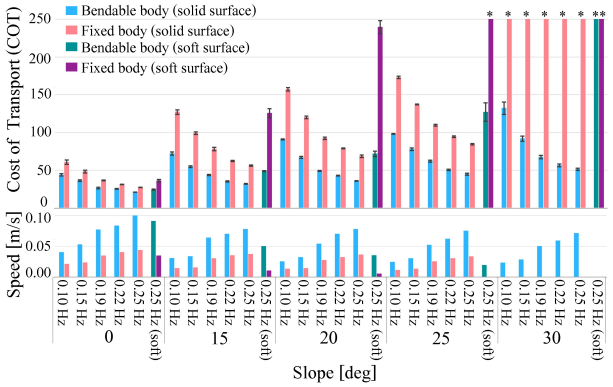

Fig. 5. (a) COT and (b) climbing speed are being compared between movements with bendable and fixed body modes on various solid and soft slopes (0, 15, 20, 25, and 30 degree). "*" indicates the cases in which the robot failed to climb the inclined surfaces and resulted in a COT > 250.

C. Ground reaction force analysis

To explain why Slalom archived a higher slope angle when it coordinates periodic lateral body flexion and limb movements during climbing. We investigated the interaction forces between the robot and the environment, and quantified them by comparing the GRFs between the robot with and without the bendable body. The results of the GRF analysis are presented in Fig. 6; when Slalom moves with a lateral undulation of the bendable body, the lateral peak force (F_x) was -2 N (see (a) in Fig. 6), and the forelimb of robot is pushed outward from the body. The force gradually increases until it reaches the medio peak force (F_x) of 4 N (see (b) in Fig. 6), suggesting that Slalom pulled its forelimb inward toward the body. Although the forelimb slips (see (c) in Fig. 6) in the case with the bendable body, it can quickly recover to a normal stance. This indicates that the forelimbs make a significant effort to prevent the robot's head from moving sideways in the second half of the stance phase. Typically, a larger medio force provides higher protection of the Slalom's head tilting out in order to maintain the movement while stepping forward. In this case, the bendable-body robot exhibited larger medio force than the fixed-body robot (see (b) in Fig. 6).

Furthermore, the GRFs illustrate that most of the propulsion in the robot is generated by its hindlimbs, as indicated by the posterior forces (F_y). More specifically, the robot with the bendable body has shown the posterior peak force of 6 N (see (e) in Fig. 6) for the hindlimbs while the forelimbs always produce a force below 4 N (see (d) in Fig. 6). Moreover, the climbing experiments with the bendable body produced approximately 3 N larger posterior forces in the hindlimbs (left hindlimb) than that with the fixed body during $45\% - 65\%$ of the stance phase (see (e) in Fig. 6). Normally, the limbs generate a positive posterior force when the robot propels itself forward by pushing the limbs backward. It is evident that the larger the value of posterior force, the higher the angle of slope the robot can climb.

Finally, we observed similar characteristics in the normal forces (F_z) for both the bendable and fixed bodies, where the normal forces peaked from 35% to 65% (see (f) in Fig. 6) during the stance phase for both the hindlimbs and forelimbs:

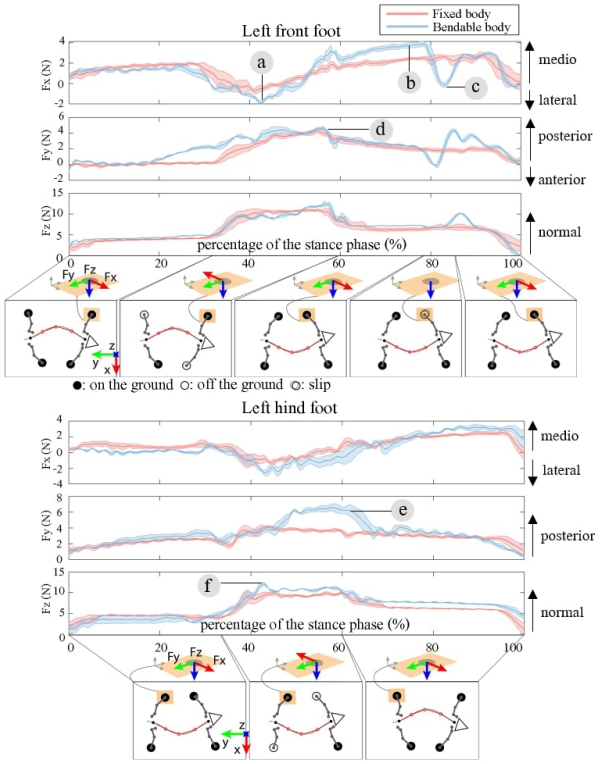

Fig. 6. Comparison of ground reaction forces (GRFs) in fixed and bendable body movements. Left forelimb and left hindlimb GRFs were measured and analysed with respect to medio-lateral (F_x), anterior-posterior (F_y) and normal (F_z). The robot with the bendable body produces medio-lateral forces in the forelimb, including (a) lateral peak force, (b) medio peak force, and (c) lateral force during slip. For anterior-posterior forces, the forelimb always produces a posterior force below 4 N (d) while the force reaches 6 N (e) for the hindlimb. The normal forces of both the bendable and fixed bodies are similar (f). Each snapshot below show the body postures and the position of feet on/off the ground during climbing.

however, larger fluctuations in force amplitude were observed with the bendable body. This indicates that the diagonal limbs have to bear most of the load in the middle of the stance phase.

D. Bending angular momentum

Based on the robot's movement dynamics caused by the continuous action of the ground reaction force, we introduce the bending angular momentum (L_{AM}) to reveal the contribution of the forelimb, hindlimb and body for maintaining the robot's movement. Mathematically, L_{AM} is defined as Equation (5) using the center of mass (COM) of the robot as the center of the bending moment.

$$L_{AM} = \left| \int_0^{T_s} -\vec{c} \times \vec{F}_{HP} \mathrm{d}t + \int_0^{T_s} -\vec{d} \times \vec{F}_{HL} \mathrm{d}t + \int_0^{T_s} (\vec{a} - \vec{c}) \times \vec{F}_{FP} \mathrm{d}t + \int_0^{T_s} (\vec{b} - \vec{d}) \times \vec{F}_{FL} \mathrm{d}t \right|, \tag{5}$$

where T_s is the duration of the stance phase, the medio-lateral and anterior-posterior forces are produced by the hind foot (F_{HL} and F_{HP}) and the front foot (F_{FL} and F_{FP}). The medio-lateral (a) and anterior-posterior (b) distances between the left and right support feet, the medio-lateral (c) and anterior-posterior (d) distances between the COM and the hind support feet are demonstrated with by similar diagrams of animals and robots in Figs. 7a and 7b, respectively. Generally,

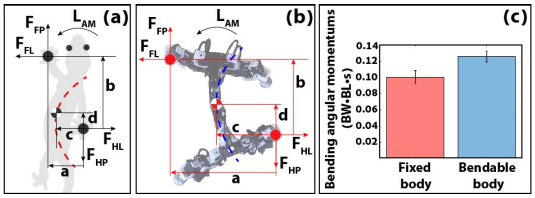

Fig. 7. A bending angular momentums is induced by GRFs during a step. (a) Gecko and (b) robot diagram of the calculation for bending angular momentum, where the center of mass was used as the center of the bending moment to calculate the bending angular momentum generated by the feet. (c) Comparison between the mean values of the bending angular momentum during robot climbing with fixed and bendable bodies. BW: body weight; BL: body length.

a greater amount of L_{AM} results in higher climbing stability on an inclined slope. The stability is obtained because of the large medio and posterior forces, which cause the COM to oscillate laterally from side to side while a pair of diagonal supporting limbs contacts the ground intermittently in a stride. The center of the bending moment (Fig. 7b) demonstrates the COM dynamics, which is explained by applying the lateral leg spring (LLS) model [27]. Perturbation experiments illustrated that the sprawling posture animal LLS models self-stabilized, despite control feedback [28]. The model was stable as the medio-lateral and anterior-posterior forces produced the lateral angular momentum that incurred in leg-to-leg transitions [29].

We converted the bending angular momentum into body weight-body length-seconds (BW·BL·s) and compared the results between the robot's moment with and without the bendable body (Fig. 7c). The mean values of L_{AM} of robot climbing with the bendable body is 0.125, which is approximately 25% higher than that of the fixed body. This indicates that the lateral undulation of the bendable body during climbing contributes not only to a transition of forces between the forelimbs and hindlimbs, but also to maintaining stability for continuity of the locomotion due to the gains of bending angular momentum. It is evident that the bendable body is used to archive the ability to climb surfaces with higher inclinations, similar to the case of geckos when climbing up slopes. To maintain their movement, they bend the spine to increase the bending angular momentum when the slope increases [30].

V. Discussion and Conclusion

We presented a systematic way to design the bendable body of a gecko-inspired robot, which is based on an experiment involving a high-speed camera recording of the movement of a Gekko gecko. The body movements of a gecko were analyzed to determine the optimal number of body joints. We used a bio-inspired approach to construct Slalom, a gecko-like robot with three body joints and four joints at each leg (19 DOFs in total) to emulate the sequence of gecko postures. CPG-based neural control with a neuromodulation (MI) was introduced to control the moving gait of Slalom. This control model is directly inspired by the biological findings and is well suited for generating a trot gait at different frequencies.

This study also demonstrated the climbing abilities of a gecko-inspired robot with lateral undulation of the bendable body. We performed a series of climbing experiments to evaluate the robot performance with and without the bendable body. The results show that the optimal locomotion speed of Slalom is at the highest stride frequency (0.25 Hz).

Moreover, it was shown that there are two reasons why a bendable body is advantageous compared to a fixed body in term of energy efficiency and efficient climbing. First, the COT of the bendable body was approximately 52% (54%) lower than that of the fixed body for all solid (soft) slopes when the robot moved at the same stride frequency (Fig. 5). Second, Slalom with the bendable body can climb a steeper slope (Fig. 5). For instance, it was unable to climb with the fixed body at a 30-degree solid slope and a 25-degree soft slope. This is because, when the angles of the solid and soft slopes were greater than 25 and 20 degrees, respectively, it began to slip on the solid slope and to get stuck on the soft slope (see http://www.manoonpong.com/Slalom/Video1.mp4).

GRF analysis demonstrated that the robot's hindlimbs generated most of the propulsion, as indicated by the posterior forces. The medio forces indicated that the forelimbs prevented the robot's head from moving sideways. The bendable-body robot exhibited greater hindlimb posterior force and forelimb medio force than the fixed-body robot. This enhanced the robot's stability while climbing steeper slopes. We calculated the bending angular momentum that resulted from the forces acting on the feet. The bendable-body robot produced a larger angular momentum, which was essential for stability during climbing. Here, the robot produced almost similar L_{AM} for all the inclined slopes where the bending radius of the bendable body was constant. In the future, we will investigate the change of bending radius to increase L_{AM} when encountering an increased slope angle, as observed in geckos [30].

Compared to existing salamander and gecko-like robots [12], [13], [14], [15], [16], [17], [20] (Fig. 8), the existing robots were designed with different structure in order to approach animal locomotor skills. Salamander robots were developed with a bendable body and leg structure with simple point-contact elements of the foot, while most of the gecko robots were constructed with an oversimplified fixed body and a complex leg structure with a special foot design with an adhesive material. In this study, Slalom has a bendable body like most salamander robots and a complex gecko-based leg structure with four DOFs and a flat foot with a passive ankle at each leg. This ankle and foot design will allow us to later implement a bio-inspired dry adhesive material with a mushroom-shaped microstructure, like other gecko robots, for energy-efficient climbing of highly inclined slopes and walls. In principle, our robot design bridges the gap between the salamander and gecko-like robots.

Regarding control mechanisms (Fig. 8), most of these salamander and gecko-like robots use inverse kinematics (IK) [15], [16], [17], [20] (requiring a robot kinematic model) or/and complex multiple CPGs [12], [13], [14] (requiring a synchronization mechanism between CPGs) to generate robot gaits with C-shaped standing and/or S-shaped traveling waves. However, our simple and single CPG-based control approach neither requires a kinematic model nor a CPG synchronization to generate a trot gait with a C-shaped standing wave. In

Robot	Control method	Multi-segmented body	Limb structure (can use adhesive material)	Locomotion modes			Surface		
				Horizontal	Slope	Vertical	Solid	Soft	Liquid
Our robot (Slalom)	CPG	✓	✓	✓	✓	✗	✓	✓	✗
Nyxrobot	IK	✗	✓	✓	✓	✗	✓	✗	✗
Stickybot	IK, Force-based controller	✗	✓	✗	✗	✓	✓	✗	✗
Gecko-inspired climbing robot	IK, Open loop controller	✗	✓	✗	✗	✓	✓	✗	✗
Gecko-inspired robot	IK, Open loop controller	✗	✓	✗	✗	✓	✓	✗	✗
Salamandra robotica I	CPGs	✓	✗	✓	✗	✗	✓	✗	✓
Salamandra robotica II	CPGs	✓	✗	✓	✗	✗	✓	✗	✓
Pleurobot	CPGs, IK	✓	✗	✓	✗	✗	✓	✗	✓

Fig. 8. A comparison between our robot (Slalom) and the other state-of-the-art sprawling posture robots (Nyxrobot [15], Stickybot [17], Gecko-inspired climbing robot [16], Gecko-inspired robot [20], Salamandra robotica I [12], Salamandra robotica II [13], Pleurobot [14]). IK: Inverse kinematics.

the future, we will extend our single CPG-based control with delay lines and premotor neural networks with a fast learning mechanism [31] to automatically obtain multiple gaits and various body patterns (standing and traveling waves). This extension will allow the robot to efficiently achieve different locomotion modes, such as walking, swimming, and climbing (up and down on inclined surfaces and walls). We will apply adaptive muscle models [32] to encode an elastic property resembling a real gecko-like flexible body.

VI. Acknowledgment

We thank Stanislav Gorb for fruitful discussions, Pongsiri Borijindakul for experimental support, and Sun Tao for comments. This work was supported by NSFC (Grant No. 51861135306) [PM, AJ] and the National Key R&D Program of China (2020YFB1313504)[PM].

References

[1] A. Zaaf, R. Van Damme, A. Herrel, and P. Aerts, "Spatio-temporal gait characteristics of level and vertical locomotion in a ground-dwelling and a climbing gecko," *Journal of Experimental Biology*, 2001.

[2] K. Karakasiliotis and A. J. Ijspeert, "Analysis of the terrestrial locomotion of a salamander robot," in *2009 IEEE/RSJ International Conference on Intelligent Robots and Systems*, Oct. 2009, pages 5015–5020.

[3] W. Nam, T. Seo, B. Kim, D. Jeon, K.-J. Cho, and J. Kim, "Kinematic analysis and experimental verification on the locomotion of gecko," *Journal of Bionic Engineering*, pages 246–254, 2009.

[4] K. Autumn, S. T. Hsieh, D. M. Dudek, J. Chen, C. Chitaphan, and R. J. Full, "Dynamics of geckos running vertically," *Journal of Experimental Biology*, volume 209, number 2, pages 260–272, 2006.

[5] J. J. Chen, A. M. Peattie, K. Autumn, and R. J. Full, "Differential leg function in a sprawled-posture quadrupedal trotter," *Journal of Experimental Biology*, volume 209, number 2, pages 249–259, 2006.

[6] D. I. Goldman, T. S. Chen, D. M. Dudek, and R. J. Full, "Dynamics of rapid vertical climbing in cockroaches reveals a template.," eng, *J Exp Biol*, volume 209, number Pt 15, pages 2990–3000, Aug. 2006.

[7] W. Wang, S. Wu, P. Zhu, and R. Liu, "Analysis on the dynamic climbing forces of a gecko inspired climbing robot based on gpl model," in *2015 IEEE/RSJ International Conference on Intelligent Robots and Systems (IROS)*, Sep. 2015, pages 3314–3319.

[8] W. Wang, A. Ji, Z. Dai, G. Qin, X. zhang, T. Ren, and Q. Han, "Angular variables of climbing geckos in two lateral undulation patterns," *Zoology*, page 125 892, 2020.

[9] R. Breithaupt, J. Dahnke, K. Zahedi, J. Hertzberg, and F. Pasemann, "Robo-salamander - an approach for the benefit of both robotics and biology," 2002.

[10] B. Chong, Y. Aydin, C. Gong, G. Sartoretti, Y. Wu, J. Rieser, H. Xing, J. W. Rankin, K. Michel, A. G. Nicieza, J. Hutchinson, D. Goldman, and H. Choset, "Coordination of back bending and leg movements for quadrupedal locomotion," in *Robotics: Science and Systems*, 2018.

[11] A. A. M. Faudzi, M. R. M. Razif, G. Endo, H. Nabae, and K. Suzumori, "Soft-amphibious robot using thin and soft mckibben actuator," in *2017 IEEE International Conference on Advanced Intelligent Mechatronics (AIM)*, 2017, pages 981–986.

[12] A. J. Ijspeert, A. Crespi, D. Ryczko, and J.-M. Cabelguen, "From swimming to walking with a salamander robot driven by a spinal cord model," *Science*, volume 315, number 5817, pages 1416–1420, 2007.

[13] A. Crespi, K. Karakasiliotis, A. Guignard, and A. J. Ijspeert, "Salamandra robotica ii: An amphibious robot to study salamander-like swimming and walking gaits," *IEEE Transactions on Robotics*, volume 29, number 2, pages 308–320, 2013.

[14] K. Karakasiliotis, R. Thandiackal, K. Melo, T. Horvat, N. K. Mahabadi, S. Tsitkov, J. M. Cabelguen, and A. J. Ijspeert, "From cineradiography to biorobots: An approach for designing robots to emulate and study animal locomotion," *Journal of The Royal Society Interface*, volume 13, number 119, page 20 151 089, 2016.

[15] D. Shao, J. Chen, A. Ji, Z. Dai, and P. Manoonpong, "Hybrid soft-rigid foot with dry adhesive material designed for a gecko-inspired climbing robot," in *2020 3rd IEEE International Conference on Soft Robotics (RoboSoft)*, 2020, pages 578–585.

[16] A. Ji, Z. Zhao, P. Manoonpong, W. Wang, G. Chen, and Z. Dai, "A bio-inspired climbing robot with flexible pads and claws," *Journal of Bionic Engineering*, volume 15, number 2, pages 368–378, 2018.

[17] S. Kim, M. Spenko, S. Trujillo, B. Heyneman, D. Santos, and M. Cutkosky, "Smooth vertical surface climbing with directional adhesion," *IEEE Transactions on Robotics*, volume 24, pages 65–74, 2008.

[18] O. Unver and M. Sitti, "A miniature ceiling walking robot with flat tacky elastomeric footpads," in *2009 IEEE International Conference on Robotics and Automation*, 2009, pages 2276–2281.

[19] Y. Liu, H. Kim, and T. Seo, "Anyclimb: A new wall-climbing robotic platform for various curvatures," *IEEE/ASME Transactions on Mechatronics*, volume 21, number 4, pages 1812–1821, 2016.

[20] M. P. Murphy, C. Kute, Y. Mengüç, and M. Sitti, "Waalbot ii: Adhesion recovery and improved performance of a climbing robot using fibrillar adhesives," *The International Journal of Robotics Research*, volume 30, number 1, pages 118–133, 2011.

[21] Z. Wang, Z. Wang, Z. Dai, and S. Gorb, "Bio-inspired adhesive footpad for legged robot climbing under reduced gravity: Multiple toes facilitate stable attachment," *Applied Sciences*, page 114, 2018.

[22] W. Wang, A. Ji, P. Manoonpong, H. Shen, J. Hu, Z. Dai, and Z. Yu, "Lateral undulation of the flexible spine of sprawling posture vertebrates," *Journal of Comparative Physiology A*, volume 204, number 8, pages 707–719, Jul. 2018.

[23] P. Manoonpong, U. Parlitz, and F. Wörgötter, "Neural control and adaptive neural forward models for insect-like, energy-efficient, and adaptable locomotion of walking machines," *Frontiers in Neural Circuits*, volume 7, page 12, 2013.

[24] W. Paulus and J. C. Rothwell, "Membrane resistance and shunting inhibition: Where biophysics meets state-dependent human neurophysiology.," eng, *J Physiol*, pages 2719–2728, 2016.

[25] D. M. Wilson, "Insect walking," *Annual Review of Entomology*, volume 11, number 1, pages 103–122, 1966.

[26] K. Mombaur, H. Vallery, Y. Hu, J. Buchli, P. Bhounsule, T. Boaventura, P. M. Wensing, S. Revzen, A. D. Ames, I. Poulakakis, and A. Ijspeert, "Chapter 4 - control of motion and compliance," in *Bioinspired Legged Locomotion*, Butterworth-Heinemann, 2017, pages 135–346.

[27] J. Schmitt and P. Holmes, "Mechanical models for insect locomotion: Dynamics and stability in the horizontal plane i. theory," *Biological Cybernetics*, volume 83, number 6, pages 501–515, 2000.

[28] T. M. Kubow, "The role of the mechanical system in control: A hypothesis of self-stabilization in hexapedal runners," *Philosophical Transactions of the Royal Society B: Biological Sciences*, volume 354, number 1385, pages 849–861, May 1999.

[29] J. Schmitt, M. Garcia, R. C. Razo, P. Holmes, and R. J. Full, "Dynamics and stability of legged locomotion in the horizontal plane: A test case using insects," *Biological Cybernetics*, volume 86, number 5, pages 343–353, 2002.

[30] Z. Wang, L. Cai, W. Li, A. Ji, W. Wang, and Z. Dai, "Effect of slope degree on the lateral bending in gekko geckos," *Journal of Bionic Engineering*, volume 12, number 2, pages 238–249, 2015.

[31] M. Thor, T. Kulvicius, and P. Manoonpong, "Generic neural locomotion control framework for legged robots," *IEEE Transactions on Neural Networks and Learning Systems*, pages 1–13, 2020.

[32] C. V. Huerta, X. Xiong, P. Billeschou, and P. Manoonpong, "Adaptive neuromechanical control for robust behaviors of bio-inspired walking robots," in *Neural Information Processing*, Cham: Springer International Publishing, 2020, pages 775–786.